



Low-velocity impact response of layered frusta tube structures

Vivek Patel¹ · Gaurav Tiwari¹ · Ravikumar Dumpala¹

Received: 25 August 2021 / Accepted: 27 December 2021 / Published online: 8 January 2022
© The Author(s), under exclusive licence to The Brazilian Society of Mechanical Sciences and Engineering 2022

Abstract

An experimental and numerical investigation was carried out to know the crashworthiness performance of layered frusta tube structures against axial impact loading. The configuration of AA-1080 frusta tubes was varied as single, double, triple and four layers, whereas the mass and velocity of the impactor were kept 20 kg and 6.7 m/s, respectively. For three-dimensional finite element analysis, commercial code Ansys/Ls-Dyna was employed and experiments were carried out through drop weight impact tester. The failure modes obtained through experiments and numerical simulations were compared and found similar for different multiwall frusta structures. The different configurations of layered frusta tubes were evaluated based on crashworthiness parameters in terms of peak force (PF), mean force (MF), crushing load efficiency (CLE) and energy absorption capability (EAC). Moreover, a parametric analysis was carried out by maintaining a constant taper angle of 5.71° with a slight variation in height, thickness, diameter and mass of impactor to analyze the dynamic response of layered frusta tube structures. The volume of all sets of layered frusta tube structures was kept approximately the same. Compared to double- and four-layered frusta tubes, the three-layered frusta tube proved to be more efficient against dynamic loading condition.

Keywords Drop weight impact · Layered frusta · Crashworthiness · Ansys · Ls-dyna · Energy absorption

1 Introduction

Safety issue has become the most prominent factor in designing of the vehicles with the rapid development of high-speed and high-power engines. In this context, the structures with lightweight material have been developed by researchers and engineers from last few decades and their crashworthiness parameters have been explored. Crashworthiness is the characteristics of the structures due to which the impact energy dissipates by deforming their own shape and thus reduces the risk of serious injuries [1].

The thin-walled tubular structures have drawn major attention of the researchers wherein the structures with varying cross section, materials, thickness, length and their physical properties have been studied against static as well as dynamic loading [2–7]. Further, the response of the structures has been addressed with controlled plastic deformation

by introducing additional geometric features (grooves and slots in radial or axial directions) [8–12].

There are several studies published in literature that explore the deformation mechanics of thin walled component against quasi-static loading where the effect of inertia was not considered in the analysis. In the case of dynamic loading due to the existence of inertia and strain rate effect, the collapse behavior of the structure was found different. The strain rate effect was studied in order to explore the crushing response of cylindrical tube made of aluminum and steel with variation in geometric parameters and impact velocity [13]. The obtained results showed that the effect of dynamic loading on steel tube was higher compare to the aluminum tube because of the material strain rate sensitivity effect. The Alexander modified analytical model [14] that derived with the influence of strain rate sensitivity factor was used to predict the mean crushing load.

The main purpose of the collapsible energy absorber is to protect the occupants by deforming its own structure during the collision. These systems are often used in high-risk areas when there is a risk of human damage to the property. In published literature, the structure was used in the form of uniform circular and rectangular cross section. Despite it, few literatures emphasized the functioning of

Technical editor: by João Marciano Laredo dos Reis.

✉ Vivek Patel
vivekmanit0031@gmail.com

¹ Visvesvaraya National Institute of Technology,
Nagpur 440 010, India

frusta tube as an energy absorber. The frusta tube is in the form of non-uniform tubular structure, i.e., varying cross section throughout the length that help the structure to deform in stable manner along with that absorb the maximum amount of impact energy.

As there are many energy absorber structures, the hollow tube uniform structure (various cross sections—circular, rectangular, square, etc.) has prominent advantageous over other available structures. A hollow tube having circular cross section is the first preference in automobiles because of its ease of manufacturing.

Apart from the uniform structure (faces parallel to the longitudinal axis), the taper structure (faces inclined towards the longitudinal axis) was also discussed by the researchers. Fig. 1b shows circular frusta which having an infinite number of tapered edges. Such structures have been considered preferable to straight (un-tapered tubes) since it provides a desirable constant mean crush load–deflection response under both axial and oblique impact loading [15]. Since the deformation behavior of frusta under oblique condition differs significantly from the axial condition, there is more scope of research in this field. Various designing parameters like semi-apical angle, thickness, upper and lower diameter and height are considered while designing. Figure 1a and b shows a schematic of circular frusta tube and fabricated frusta tube, respectively.

The frusta having a circular cross section provided a uniform load–displacement curve compared to the energy absorber such as circular, rectangular, pyramidal, hexagonal and triangular [16]. The gradual varying cross-sectional area of the structure influenced their energy absorption capability. Further at the time of the impact, the taper tubes produced less inertia effect [14] which helped to minimize the Euler-buckling deformation mode

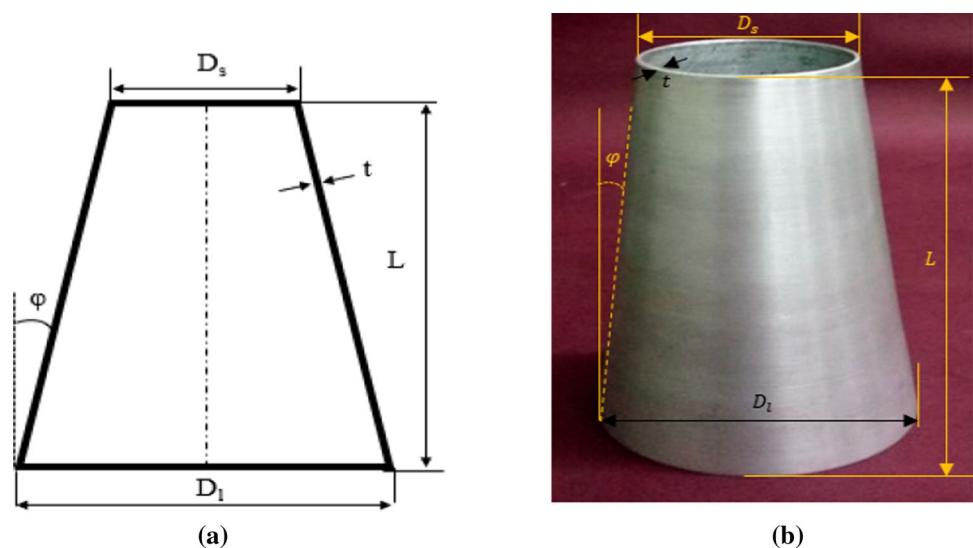
Prasad and Gupta [17] analyzed large angle frusta against both quasi-static and dynamic loading conditions. The load displacement plot and the collapse behavior of frusta were found similar for both loading conditions, whereas for the dome shell it was different as different strain rates. With an increase in the slenderness ratio, the energy absorption and the mean load of the frusta tube increased.

Sobky et al. [18] investigated the effect of constraint provided in frusta tube under impact loading condition. For analysis four constrained structures were developed such as: (i) top constrained, (ii) bottom constrained, (iii) completely constrained and (iv) non-constrained frusta. The top end constrained frusta tubes offered highest specific energy absorption.

Recently, multicell [19–21] and multiwall [22] tubes have been found to be of great interest due to its higher energy-absorbing capability in low-volume structure. Kim [19] explored a multicell profile having a four-square cell at the corner and found the improvement in crushing performance. In the same context, Mahmoodi et al. [20] studied the tapered thin walled tubes having multicorner and multicell configurations. It was found that crashworthiness performance of such structure indicated a strong reliance on the geometry and cross section of the structure. Gan et al. [21] investigated the crushing response of multifrusta configuration against the axial impact loading. The analysis was mainly focused on the column spacing, cells, number of tubes and combination of cone. It was found that a cross-arranged combination of taper tubes improves energy absorption capacity.

Kashani et al. [22] explored the response of square bi-tubular structure under the quasi-static loading condition through experimental and numerical investigation. The bi-tubular structure with two configurations of inner tube (diamond and parallel) was studied to predict the energy

Fig. 1 a Schematic representation of frusta tube and b fabricated frusta tube



absorption capacity. The energy absorption in a parallel configuration was up to 8% more than the sum of the energy absorbed by the inner and outer tubes, while it was up to 36% higher in a diamond arrangement of bi-tubular construction.

Goel [23] compared the crushing performance of bi-tubular and tri-tubular structures having both square and circular cross section with the foam filler and found that circular section enhanced the energy absorption capacity.

The development of multicell and multiwall tubular structure showed significant increase in crashworthiness performance of the structure. The reported studies mainly reported the crushing behavior of circular and rectangular multiwall and multicell tubular structures. However, the studies related to the tapered multiwall structures are very limited despite its good crashworthiness performance in crash event. In order to explore its suitability for a better energy absorber, a thorough study is therefore required.

The current work emphasized the crashworthiness performance of developed hybrid frusta tube in the form of layer (double, triple and four layers) having a circular cross section against low-velocity impact loading. The work focused on the deformation characteristics that obtained from both experimental and numerical analysis. Furthermore, obtained results provide a detailed comparison in terms of applied mass loading and the number of layers associated with each configuration of hybrid frusta tube structure. The different layered frusta configuration with a combination of height including double-layered (91.6 mm and 82 mm), triple-layered (91.6 mm, 86 mm and 78 mm) and four-layered (91.6 mm, 87 mm, 82 mm and 77 mm) along with the thickness

variation (2.3 mm to 0.4 mm) has been explored to identify better energy absorption structure.

2 Material and specimen

The fabricated frusta samples were made of AA-1080 through a spinning process.

The optical electron spectrography (OES) was used to determine the chemical composition of metal sheets, and the results are depicted in Table 1.

The fabricated frusta tube was developed in the form of layer as shown in Fig. 2.

2.1 Material details

In the current work, AA-1080 was used to fabricate the layered frusta tube. The main objective is to develop hybrid frusta and examine the deformation behavior against the low-velocity impact loading. As aluminum having a light-weight and less cost, the designer more focused on it and developing an energy absorbing structure that replaces the steel.

The primary reason for selecting a material as aluminum AA-1080 is that it is widely used material as an energy absorbing component and it is easily available in market. In addition to this, we chose an AA-1080 in order to provide more data for a different grade of aluminum.

The mechanical properties of the fabricated sample were determined by the INSTRON universal testing machine

Table 1 Chemical composition of AA-1080

Material	Si	Fe	Cu	Mn	Zn	Cr	Ti	Other	Aluminum
wt%	0.043	0.145	0.0017	0.0013	<0.0017	0.0013	0.025	0.0182	99.77

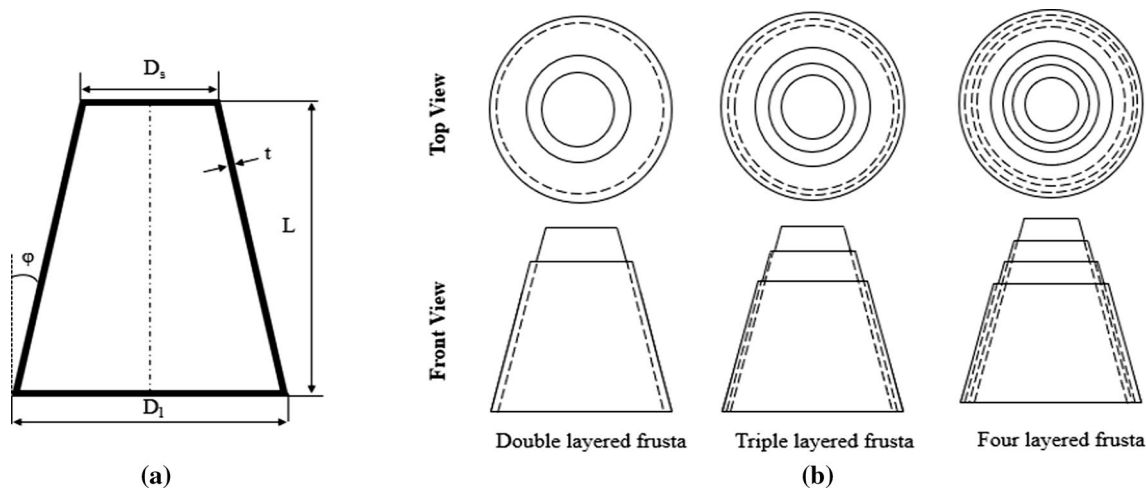


Fig. 2 Schematic representation of developed layered frusta tube

with a capacity of 30 tons at a rate of 2 mm/min. For this, two dumbbell-shaped samples were cut via wire EDM from the fabricated sample [24], which complies with the ASTE8M-98 standard. Figure 3 represents the obtained true stress–strain plot.

The mechanical properties found from the true stress–strain plot are depicted in Table 2.

2.2 Samples specifications

A total of four sets of each layered frusta tube were simulated with the same semi-apical angle as well as the same volume difference.

In order to examine the effect of thickness for each layered configuration, volume was calculated and found the difference of it. Then, the obtained volume difference of each layered was added and that has to be found approximately close to the difference of volume for monolithic frusta having thickness 2.3 mm. In the current analysis, the height, thickness and diameter (both the upper and lower ends) of the sample varied in order to preserve approximately the same volume.

The volume of specimen was calculated as:

$$V = \frac{\pi \times L}{3} (D_l^2 + D_l \times D_s + D_s^2) \quad (1)$$

2.3 Samples nomenclature

For sample identification, each one was assigned with the combination of numbers and alphabets that have a specific significance. The different frusta tubes, i.e. double-, triple- and four-layered structures, were named as W2, W3 and

Table 2 Mechanical properties of AA-1080

Property	Modulus of elasticity	Poisson's ratio	Ultimate tensile strength	Yield strength
Value	69 GPa	0.33	106.72 MPa	93.61 MPa

W4, respectively. In each layered frusta tube, four models were simulated that identified as DB1 to DB4, DT1 to DT4 and DF1 to DF4 for respective double-, triple- and four-layered structure.

3 Experimental and simulation details

3.1 Experimental details

The drop weight impact test was performed on the layered frusta tube with the impactor mass of 20 Kg. The achieved velocity of the impactor was 6.7 m/s. Figure 4 shows the drop weight impact setup which consists of one long 2-m seamless cast steel tube (HSN-7304) to provide a path for the impactor and a base on that specimen has to be kept.

The impact velocity was measured as:

$$V = \sqrt{2gh} \quad (2)$$

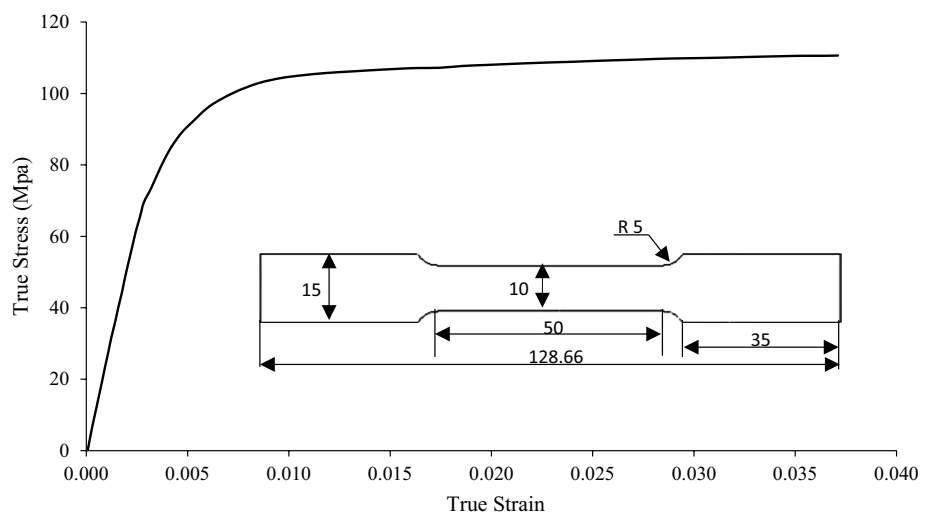
where g = gravitational acceleration

h = distance that the object travels or falls

Table 3 depicts the specification details of the double-layered (Ex_W2_DB), triple-layered (Ex_W3_DT) and four-layered (Ex_W4_DF) frusta tube.

The drop weight impact test provides the details of deformation modes of the samples mentioned in Table 3.

Fig. 3 Obtained true stress–strain curve of AA-1080 [24]



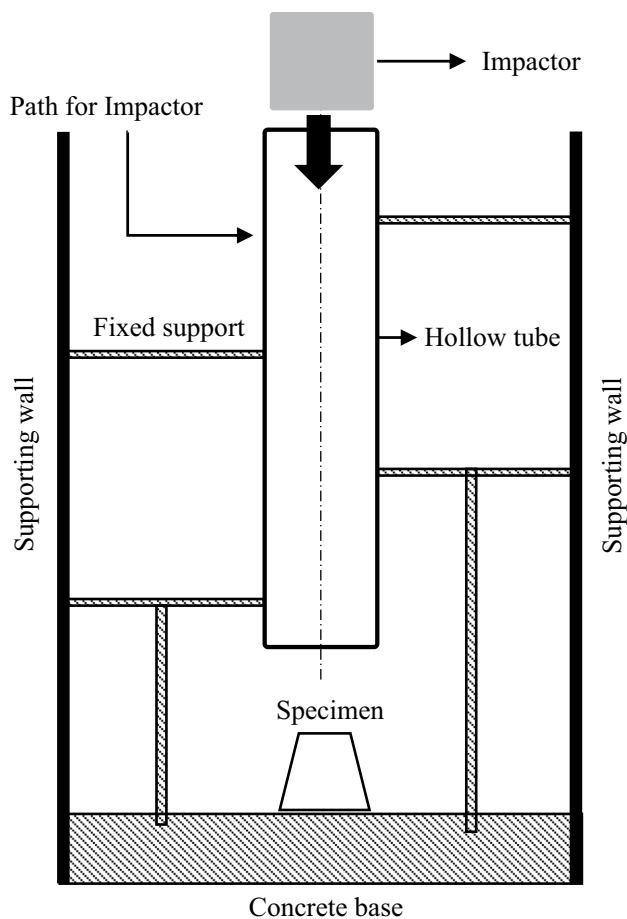


Fig. 4 Schematic view of drop weight impact test

3.2 Numerical modelling details

The nonlinear finite element software Ansys-LS-Dyna was used to simulate and explored the crashworthiness performance of the layered frusta tube against impact loading. In simulation impactor mass varied as 20 kg, 30 Kg and 40 Kg, in order to evaluate the collapse behavior of layered frusta tubes at different impactor mass. The simulated model comprised with the one top rigid plate, deformable frusta structure and lower rigid plate. During assigning contacts, top rigid plate was considered as master and frusta structure was assigned as slave surfaces. The slave body assigned as the Belytschko–Tsay shell element (four-node shell element), and the master surface was considered as solid. The velocity was assigned to upper rigid plate, whereas bottom rigid plate was constrained in all the directions. The *Mat24-piecewise linear plasticity* material model was assigned to the layered frusta, and the *Mat20-rigid* was considered for the rigid plate. The *automatic surface to surface contact* was established between layered frusta and the rigid plate as well as between the frusta layers. The *automatic single surface contact* (acting as self-contact) was assigned to the

tube in order to avoid the interpenetration between the tubes, as folding progresses during the impact loading.

The optimum mesh size was obtained through a mesh convergence study. Vivek et al. [25] studied different mesh sizes (0.8, 1.2, 1.5, 2 and 2.5) and simulate the double-layer frusta tube. The obtained peak force (PF) was compared with the experimental results. The PF for the mesh size of 1.2 mm was close to the value obtained through experimental results. Further, the percentage error of PF value was minimum for the mesh size of 1.2 mm. Therefore, it is considered as optimum mesh size for further simulation.

In the simulation, the body which is deforming by the means of folding creates a chance to penetrate the successive layer or the boundary and affects the results and deformation pattern. Therefore, in order to avoid such condition two friction coefficients, i.e. dynamic and static, have to define in the keyword *Contact*. Chahardoli and Nia [26] studied number of values and found that 0.3 and 0.2 (taken as dynamic and static coefficient of friction) provide a good agreement between the numerical and experimental value. Therefore, in the current study the value of static and dynamic friction was assigned as 0.3 and 0.2, respectively.

The simulated sample details are shown in Table 4.

4 Result and discussion

4.1 Validation of numerical model




The primary concern before simulating the developed design was the accuracy of the numerical model. The developed sample referred in Table 3 was experimentally evaluated in the current paper using a drop weight impact test. In addition, the same loading and boundary condition was used for the numerical analysis to verify the opted numerical model with the experimental results.

In this paper the validation of numerical model was predicted based on the deformation characteristics for each layered configuration. In order to predict the accuracy in the absence of the force and displacement curve, the deformed structure was compared through its cut-section view. It provides the detail comparison of folding of each layer of double-, triple- and four-layered frusta tube. Both experimentally and numerically observed deformation was found nearly similar mode of folding that helps the reliability of the current study.

In order to provide a similar experimental condition, the mechanical properties were obtained from the uni-axial tension test and true stress–strain plot was obtained, see Table 2.

The deformation modes of double-, triple- and four-layered frusta tube structure obtained through experiments and

Table 3 Specification details of the experimentally tested layered samples

Sample	Part	Larger end Diameter (D_l) (mm)	Smaller end diameter (D_s) (mm)	Height (H) (mm)	Thickness (t) (mm)
	Inner	62.6	44.88	91.6	1.1
	Outer	65	48	85.5	1.2
	Inner	60.8	43.3	91.6	1.05
	Middle	63.3	47	85.8	1.15
	Outer	66.2	51.1	79.5	1.2
	Inner	61.3	43	91.6	1.15
	Second	63.36	46.2	87	1
	Third	65.4	49.5	82	1
	Outer	67.5	53	77	1

numerical simulations were compared in order to verify the reliability of the chosen FE models.

As the impact happens, tubular structures which act as an energy absorber deform with the formation of concertina (i.e., axisymmetric ring formation), diamond (i.e., lobes formation) and mixed mode (i.e., concertina followed by a diamond mode). In case of layered hybrid frusta tube structures, the deformation mechanism showed a new kind of deformation known as a rolling mode of deformation [25]. In this the inner layer starts to deform with the outward folding and completes one roll followed by a concertina folding.

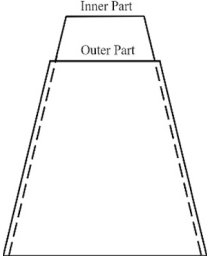
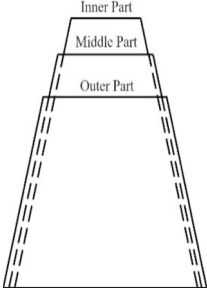
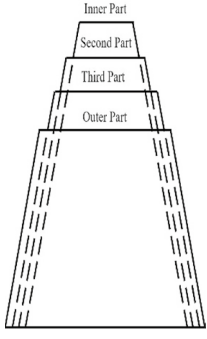
For double-, triple- and four-layered structures, the actual crushed length was 25, 22 and 18 mm, respectively, whereas corresponding numerical values were 23.8, 21.5 and 16.25 mm, respectively. The crush length obtained from actual and predicted results was close enough for particular case. Figure 5 reflects the experimentally and numerically obtained

deformation pattern of double-layered frusta and found nearly the same modes of failure, i.e., concertina folding accompanied by lobe formation initiation. It was further supported by means of a section view, see Fig. 5b, in that lobes were identified at the same location.

In case of three-layered frusta tube, the structure deformed with the initiation of the outward folding. As the deformation progressed, it formed the lobes that caused the diamond mode of failure that is shown in Fig. 6. The cut-section view (Fig. 6b) shows the diamond failure modes of all layers of frusta structures.

Further, in case of four-layered frusta tube, the layers were folding in outward direction that can be observed in Fig. 7. The cut-section view is shown in Fig. 7b; it was observed that the inner tube of both numerically and experimentally tested sample deformed with the initiation of inward folding followed by the lobes formation.

Table 4 Specification details of samples

Sample	Part	Larger end Diameter (D _i) (mm)	Smaller end diameter (D _s) (mm)	Height (L) (mm)	Thickness (t) (mm)	Volume (mm ³)		
	W2_DB1	Inner	61	42.8	91.6	1.2	32802.37	
		Outer	63.2	46.8	82	1.1		
	W2_DB2	Inner	61	42.8	91.6	1.3	32811.40	
		Outer	63	46.6	82	1		
	W2_DB3	Inner	61	42.8	91.6	1.4	32819.82	
		Outer	62.8	46.4	82	0.9		
	W2_DB4	Inner	61	42.8	91.6	1.5	32827.65	
		Outer	62.6	46.2	82	0.8		
	W3_DT1	Inner	61	42.8	91.6	0.9	32868.18	
		Middle	62.6	45.4	86	0.8		
	W3_DT2	Inner	61	42.8	91.6	1	32864.19	
		Middle	62.6	45.4	86	0.8		
	W3_DT3	Outer	63.6	48.2	78	0.5	32893.02	
		Inner	61	42.8	91.6	1.1		
	W3_DT4	Middle	62.4	45.2	86	0.7	32846.73	
		Outer	63.4	47.8	78	0.5		
		W4_DF1	Inner	61	42.8	91.6	0.8	32803.90
			Second	62.2	44.6	87	0.6	
			Third	63.2	46.6	82	0.5	
		W4_DF2	Outer	64	48.4	77	0.4	32823.51
Inner			61	42.8	91.6	0.9		
Second			62	44.6	87	0.5		
Third			63	46.6	82	0.5		
W4_DF3		Outer	63.8	48.4	77	0.4	32835.60	
		Inner	61	42.8	91.6	1		
		Second	62	44.6	87	0.5		
		Third	62.8	46.4	82	0.4		
W4_DF4		Outer	63.6	48.2	77	0.4	32776.4	
	Inner	61	42.8	91.6	1.1			
	Second	61.8	44.4	87	0.4			
W4_DF4	Third	62.6	46.2	82	0.4	32776.4		
	Outer	63.4	48	77	0.4			

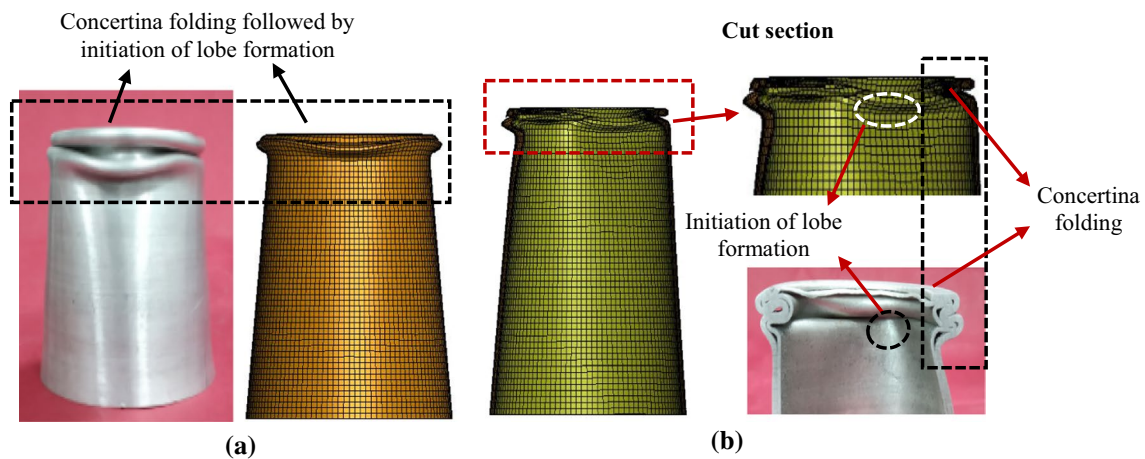


Fig. 5 Comparative analysis of experimentally and numerically obtained deformation pattern of double layered 15 frusta tube: **a** whole model, and **b** cut-section

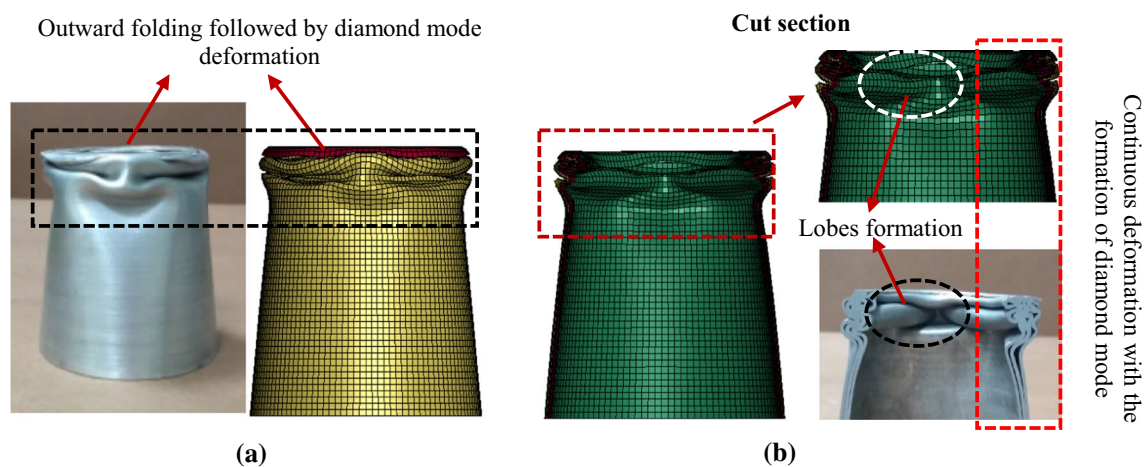


Fig. 6 Comparative analysis of experimentally and numerically obtained deformation pattern of triple-layered frusta tube: **a** whole model and **b** cut-section

The collapse modes and the behavior of folding had therefore proposed that the use of the FE model in the current investigation can be regarded as a reliable approach for evaluating the experimental examination.

4.2 Crashworthiness indicators

The capability of the structure to withstand against impact loading condition depends on the crashworthiness parameters: peak force (PF), mean force (MF), crash load efficiency (CLE) and energy absorption capacity (EAC). These parameters were extracted from the load–displacement plot of layered frusta that was obtained at a different impactor mass. The obtained results at a different impactor mass are depicted in Table 5.

The PF (initial maximum force) is not intended to reach a higher value in a very short period of time, which triggers the sudden reaction force felt by the occupant or the survival object. Therefore, PF is considered as a very significant parameter that describes the performance of the structure along with the deformation behavior.

In the current analysis, the layered frusta tube was analyzed with a constant velocity of 6.7 m/s against the range of impactor mass (20, 30 and 40 Kg). A maximum PF was observed for the double-layered frusta tube compared to three- and four-layered configurations against all the masses.

The different sets of double-layer frusta tubes showed significantly higher variation in PF and found that the range was 19.54–28.18 KN, 18.75–28.47 KN and 20.39–28.27 KN for 20, 30 and 40 Kg impactor weights, respectively.

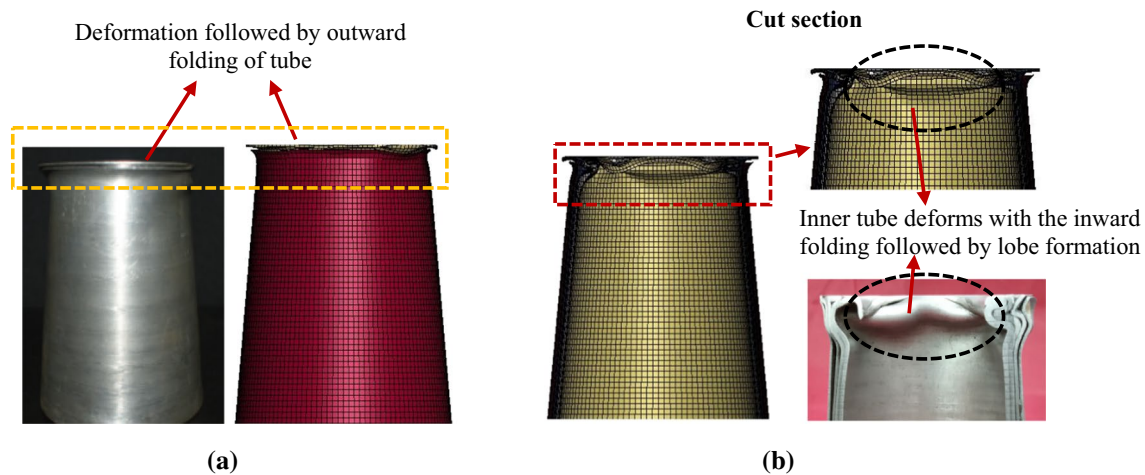


Fig. 7 Comparative analysis of experimentally and numerically obtained deformation pattern of four layered frusta tube: **a** whole model and **b** cut-section

From these variations, it was concluded that the double-layered structure showed inconsistency in achieving the initial PF that directly affects the performance of the structure.

In the same manner, for triple-layered frusta structure, the variation of PF was found as 17.67 - 20.88 KN, 18.62 - 21.09 KN and 18.65 - 19.92 KN, respectively, against 20, 30 and 40 kg impactor mass, respectively, whereas for four-layered frusta respective range was 17.34 - 18.80 KN, 17.44 - 19.14 KN and 17.39 - 19.54 KN for 20, 30 and 40 Kg impactor mass.

The MF must be close enough to the PF to have a higher CLE, which is determined by the ratio of the MF to the PF. It helps to deform the structure in stable manner that is clearly observed from the load–displacement plot of different sets of layered configurations. For different impactor mass the variation in CLE was found more for the simulated layer frusta tube. For the double-layer frusta, the CLE range was 52% to 62%, 57% to 71% and 56% to 77% for the 20, 30 and 40 Kg impactor mass, respectively. For triple-layer frusta structure, respective range of CLE was 65% to 81%, 65% to 80% and 76% to 81% and the corresponding variation for four-layered frusta was 59% to 78%, 62% to 80% and 67% to 83% obtained for the 20, 30 and 40 Kg impactor mass, respectively. In addition, the load–displacement curve stability reflects the higher EAC, as it is defined as the region under the load–displacement curve.

In simulation process the load–deformation curve was obtained that further helps to determine the energy absorbing capability (EAC) of the layered hybrid frusta tube structures. The energy was calculated by integrating the obtained simulated load–displacement curve and the higher value of EAC reflects the stability of the load–displacement curve.

4.3 Failure modes of multilayered frusta tube

Figures 8, 9 and 10 show the failures mode of double-, triple- and four-layered frusta tube structure, respectively, that undergone with different impactor mass.

As the impactor mass increased, the crushed length of layered structure increased along with change in deformation pattern. The early contact of the impactor with the structure forms a concertina mode in the case of a double layered frusta tube, which changed to diamond mode as the deformation progressed, see Fig. 8. The same behavior of double-layer frusta tube was found for all studied impactor mass. The inner tube deformed with the development of inward folding at the initial impact, which provided a plastic flow of the outer layer before the impactor actually came into contact. It caused the outward rolling mode of deformation of the outer layer.

The resistance offered by the structure was reduced as the diamond mode formed, which was directly depicted in the load–displacement plot of the double layer frusta. The unstable behavior of the load–displacement plot caused the decrease in MF, and because of this the difference in PF and MF increased, resulting in a reduction in CLE.

The three-layered frusta and four-layered frusta structure deformed in controlled manner with the formation of concertina mode for all impact loading. The steady mode of deformation enhanced the performance of the structure. The three-layered structure formed a concertina mode for all studied impact mass, indicating the stability of the structure under the dynamic impact loading condition.

For four-layered frusta structure, folding was not identical against studied impact mass. After concertina mode, some lobes were formed in case of 20 kg and 30 Kg impactor mass that led the diamond mode of deformation.

Table 5 Obtained crashworthiness parameters at different impactor mass loading

Sample	PF (KN)	MF (KN)	CLE (%)	Energy (J)
<i>Impactor mass = 20 kg</i>				
W2_DB1	28.18	15.47	0.55	433.24
W2_DB2	19.54	10.22	0.52	295.55
W2_DB3	25.62	15.17	0.59	429.06
W2_DB4	24.79	15.41	0.62	421.83
W3_DT1	18.76	14.05	0.75	400.62
W3_DT2	20.88	13.49	0.65	390.67
W3_DT3	17.67	14.29	0.81	407.42
W3_DT4	18.61	12.92	0.69	370.96
W4_DF1	18.35	13.24	0.72	380.34
W4_DF2	17.34	13.45	0.78	385.76
W4_DF3	18.80	12.81	0.68	367.14
W4_DF4	18.62	10.97	0.59	319.24
<i>Impactor mass = 30 kg</i>				
W2_DB1	27.94	16.41	0.59	621.30
W2_DB2	18.75	10.73	0.57	418.12
W2_DB3	28.47	16.95	0.60	636.27
W2_DB4	25.75	18.28	0.71	662.75
W3_DT1	19.11	14.72	0.77	567.31
W3_DT2	21.09	13.72	0.65	538.40
W3_DT3	18.62	14.82	0.80	572.60
W3_DT4	19.27	13.89	0.72	536.11
W4_DF1	18.90	13.75	0.73	533.65
W4_DF2	17.44	13.98	0.80	542.76
W4_DF3	19.14	13.59	0.71	524.65
W4_DF4	18.89	11.75	0.62	458.16
<i>Impactor mass = 40 kg</i>				
W2_DB1	25.84	16.81	0.65	806.02
W2_DB2	20.39	11.44	0.56	558.60
W2_DB3	28.27	17.44	0.62	828.42
W2_DB4	25.08	19.27	0.77	890.77
W3_DT1	18.92	15.16	0.80	737.31
W3_DT2	19.92	15.16	0.76	737.21
W3_DT3	18.65	15.19	0.81	741.46
W3_DT4	19.30	14.63	0.76	708.12
W4_DF1	19.10	14.57	0.76	708.09
W4_DF2	17.39	14.51	0.83	706.26
W4_DF3	19.54	13.97	0.71	679.74
W4_DF4	18.74	12.48	0.67	608.43

4.4 Load–deformation response of multilayered frusta

Figures 11, 12 and 13 show the load–displacement and energy–displacement plot of layered frusta tubes that examined against 20, 30 and 40 Kg impactor mass. It was observed that, among all load–displacement plots,

the simulated double-layer frusta tube showed variation throughout the deformation.

It happened because, in order to maintain the same volume, the thickness variations in the double-layer frusta tube were more than in the other layered configurations of frusta tube. Furthermore, it was found that the maximum thickness variation throughout the deformation process resulted in a higher PF, which was particularly noticeable for the double-layered frusta tube.

After reaching the maximum PF, the fall of the load reflected the formation of a plastic hinge that further initiated the folding. At the same time, the subsequent layer of the layered tube contributed to the further phase of deformation along with the impactor. The subsequent layer, other than the layer on which direct impact loading was performed, began to deform as a result of the impact wave produced during the original impact. The deformation was transmitted onto the adjacent layers, bringing the entire system to reach in a plastic state.

As the interaction of layer increased, the initial peak force decreased that can be easily observed from the load–displacement plot of triple- and four-layered structures (see Figs. 12 and 13). The inclusion of layers as the deformation progressed helped to keep the mean force (MF) close to the peak force (PF), which was not attained in the double-layered configuration.

Both the triple- and the four-layer frusta tube structures displayed stability in the load–deformation curve.

The energy–displacement curve for the double-layered frusta tube was not identical like the response of remaining layered frusta tube, see Figs. 11a, 12a and 13a. In double-layer frusta, some of the simulated model achieved a maximum stroke length but the corresponding energy absorption capacity was lower. The triple- and four-layered frusta tube illustrated the stability of the load–displacement curve; corresponding to it, energy absorption behavior represented the identical trend line.

4.5 Effect of loading and number of layers

The layered frusta tube structures were investigated against three impactor masses 20, 30 and 40 kg at a constant velocity of 6.7 m / s. The four configurations were taken for each layered frusta tube, and the average value of MF, PF, CLE and EAC is plotted in Figs. 14 and 15 against respective impactor mass. The stroke length of the layered frusta raised with increase in the number of layers of the frusta structures and impactor mass. It was observed that the stroke length increased for the same loading condition with increase in the number of layers of the frusta, see Fig. 14a. The allocated thickness of each layer was reduced with the increase in the layers and achieved a comparatively higher stroke length.

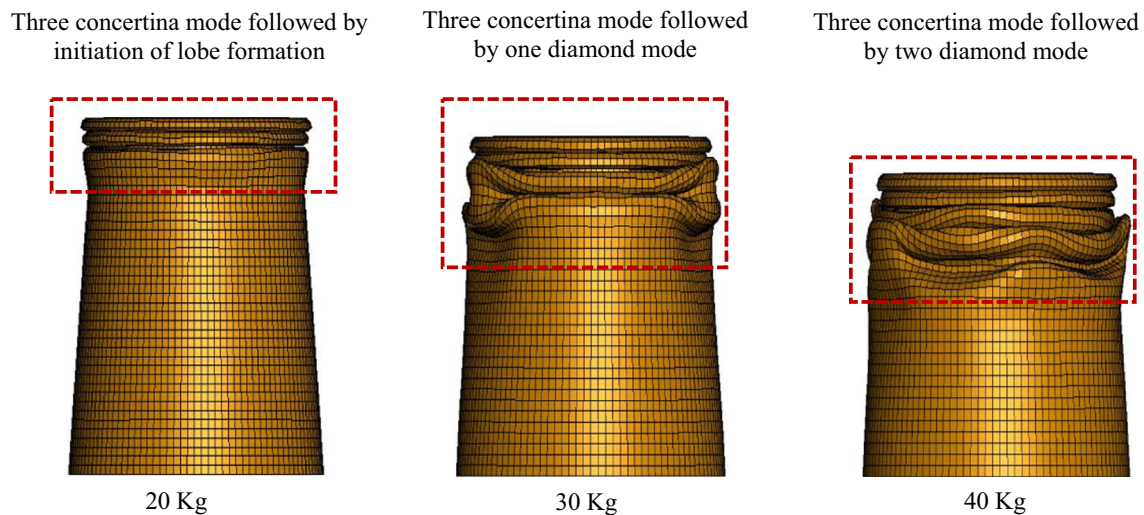


Fig. 8 Comparison of folding pattern of the double-layered frusta tube at different impactor mass

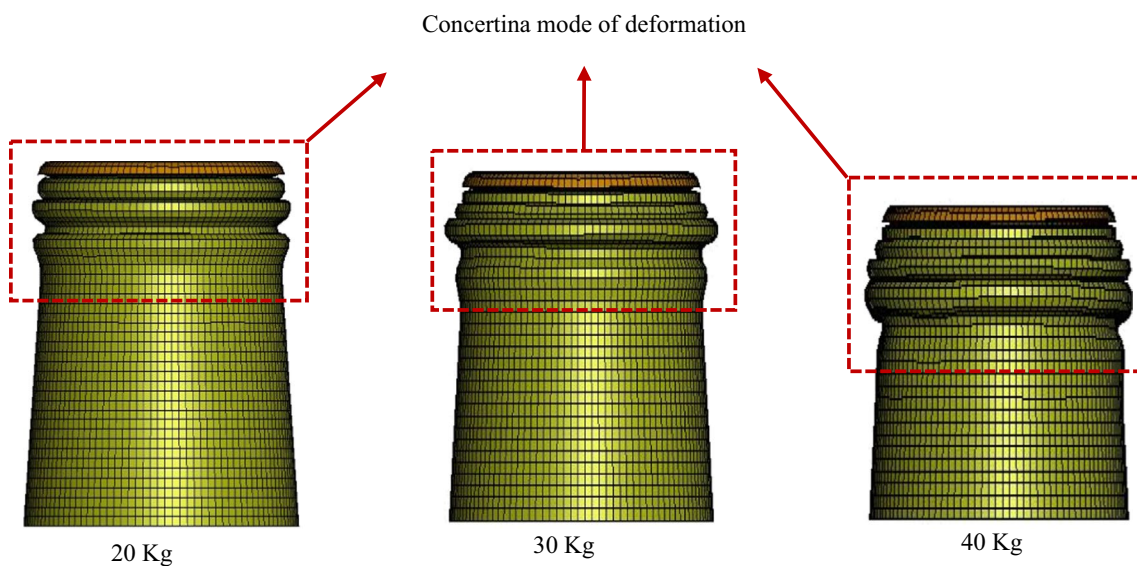


Fig. 9 Comparison of folding pattern of the triple-layered frusta tube at different impactor mass

This clearly indicated that the thickness was a significant factor for a layered configuration design.

In order to compare the energy absorption by the different layered configuration of the structure, the crushed length was kept identical against particular mass, i.e. 32 mm for the 20 Kg, 45 mm for the 30 Kg and 54 mm for the 40 Kg impactor mass. Fig. 14b shows that the energy absorption decreased with increase in the layers of the structure. It was found that when the layers increased from double to triple the EAC decreased by 0.6%, 5.3% and 5.1% for the impact mass loading of 20, 30 and 40 Kg, respectively, and further increased in layer from triple to four, EAC reduced as 7.4%, 7% and 7.5%, respectively, for 20, 30 and 40 Kg

mass loading. The reduction of the EAC was found to be a minimum for the triple layer relative to the four-layer frusta tube. Furthermore, with the increase in the layers for frusta structure, the stroke length increased for a particular mass and corresponding to the same stroke length EAC was found to be lower for all impactor mass, see Fig. 14.

At the same time, the reaction force offered by layered structure during the initial impact was decreased with the rise in number of layers for all studied impactor mass (see Fig. 15), similar to the case for quasi-static loading [25]. As layers increases from two to three, the reduction of PF was found to be nearly 23% for all impactor mass, whereas PF reduction was found to be 4% for 20 Kg, 5% for 30 Kg and

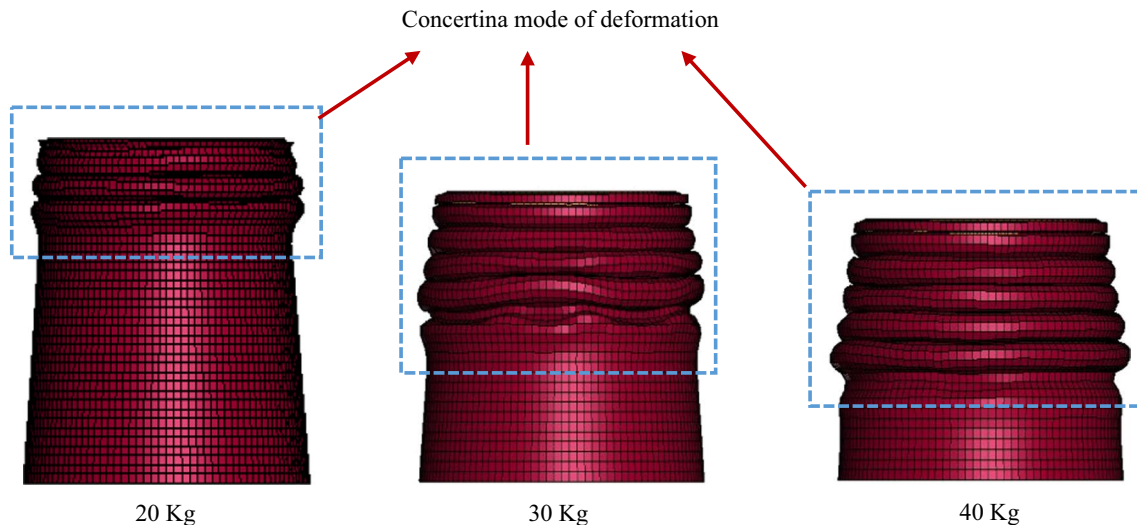


Fig. 10 Comparison of folding pattern of the four-layered frusta tube at different impactor mass

3% for 40 Kg impactor mass when layers increased from three to four (see Fig. 15a).

This implied that as the layers increased in the multiwall frusta structure, the effect of initial impact decreased that was more important for the survival of the occupant in the crumple zone. The reduction in MF was found to be less for the triple- and four-layered frusta structure compared to the double-layered frusta tubes (Fig. 15b) that affected the corresponding crash load efficiency (Fig. 15c). As the difference between PF and MF was more, the crash load efficiency was less.

5 Conclusion

In the present paper, the effect of low-velocity impact on the crashworthiness performance of double-, triple- and four-layered frusta tube structure was examined. The effect of impactor mass was analyzed based on the crashworthiness parameters. The significant findings from the present study are as follows:

- Layered configuration was affected by the thickness distribution of consecutive layers. For identical impactor,

stroke length was found to be increased with increase in number of layers in the frusta structure.

- The peak force dropped significantly as the number of layers of the frusta tubes increased, with a slight reduction in mean force. The PF reduction when the layer increases from double to triple was found to be nearly 23% for all studied impactor mass, while it reduced as 4% for 20 kg, 5% for 30 kg and 3% for 40 kg impactor mass when layer increases from three to four.
- With the increase in the layer, EAC of the structure decreased. When the number of layers increased from double to triple, it dropped as 0.6%, 5.3% and 5.1% for the impact mass loading of 20, 30 and 40 kg, respectively, and the EAC decreased by 7.4%, 7% and 7.5%, respectively, for 20, 30 and 40 kg impactor mass when the number of layers increased from triple to four in a multiwall frusta structure.
- The CLE varied from 0.52 to 0.62, 0.57 to 0.71 and 0.56 to 0.77 for double-layered, 0.65 to 0.81, 0.65 to 0.80 and 0.76 to 0.81 for triple-layered, and 0.59 to 0.78, 0.62 to 0.80 and 0.67 to 0.83 for four-layered frusta tube against 20, 30 and 40 kg impactor mass loading, respectively.

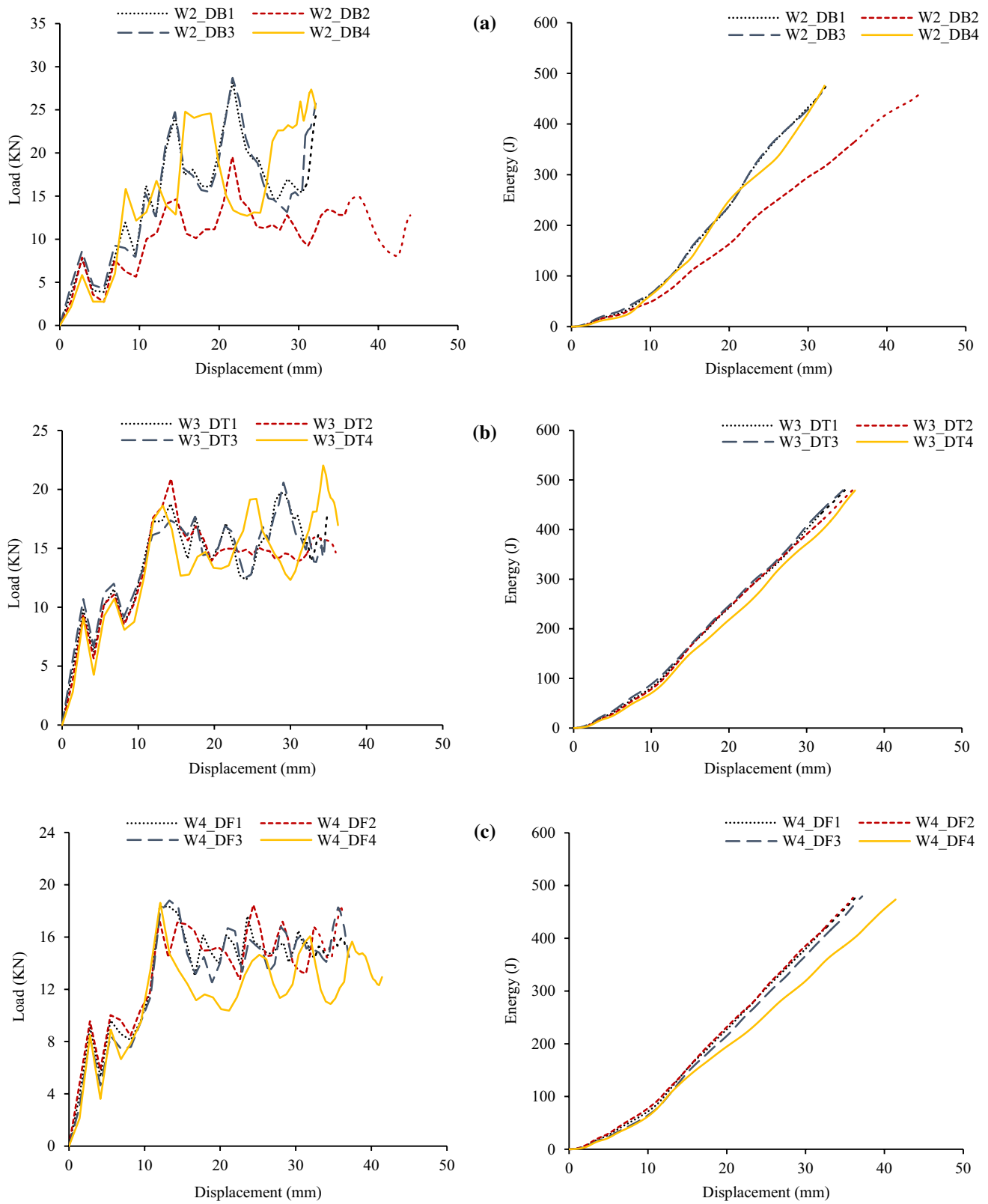


Fig. 11 Load–displacement and energy–displacement plot of: **a** double-, **b** triple- and **c** four-layered frusta tube at 20 kg impactor mass

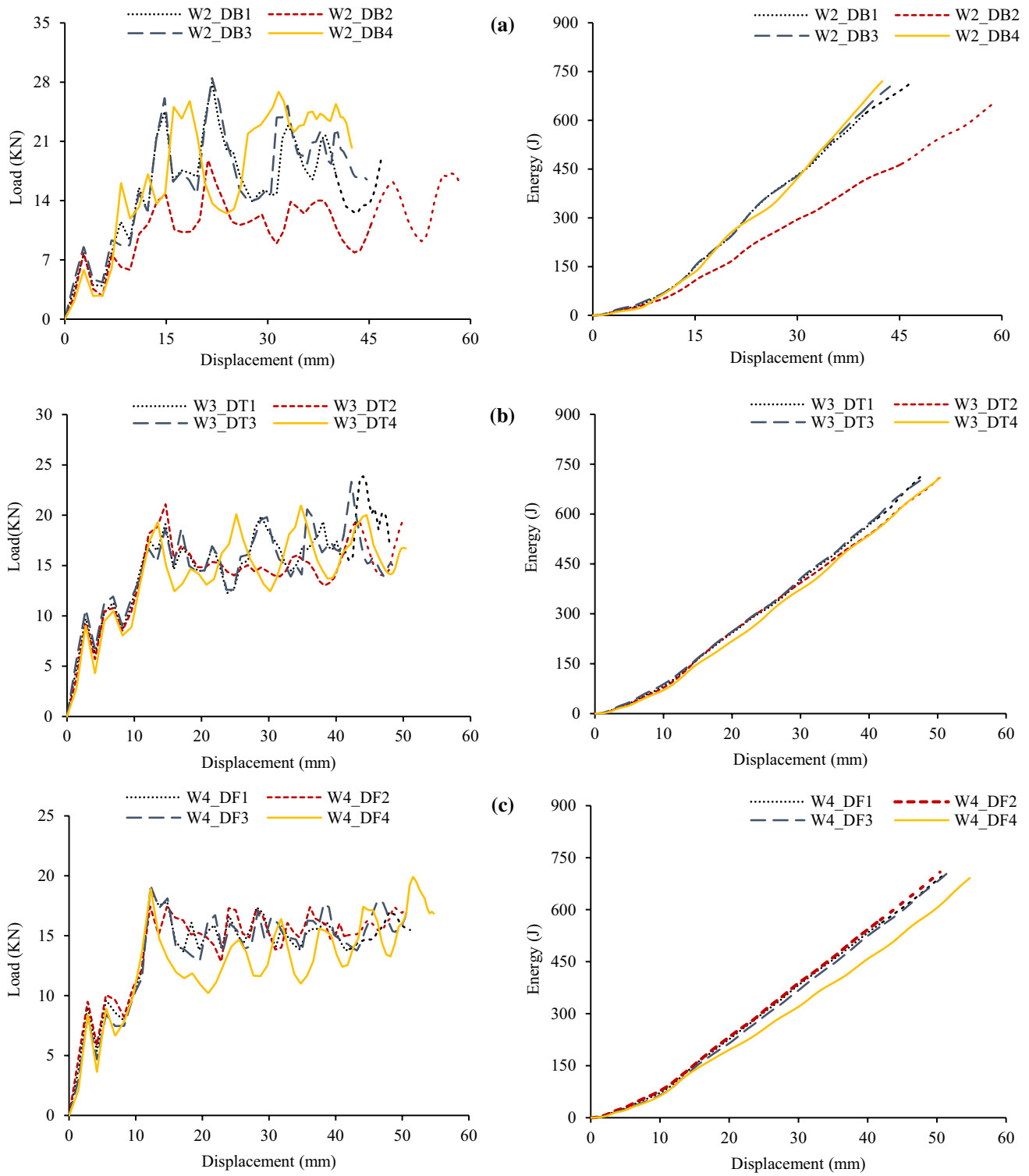


Fig. 12 Load–displacement and energy–displacement plot of: **a** double-, **b** triple- and **c** four-layered frusta tube at 30 kg impactor mass

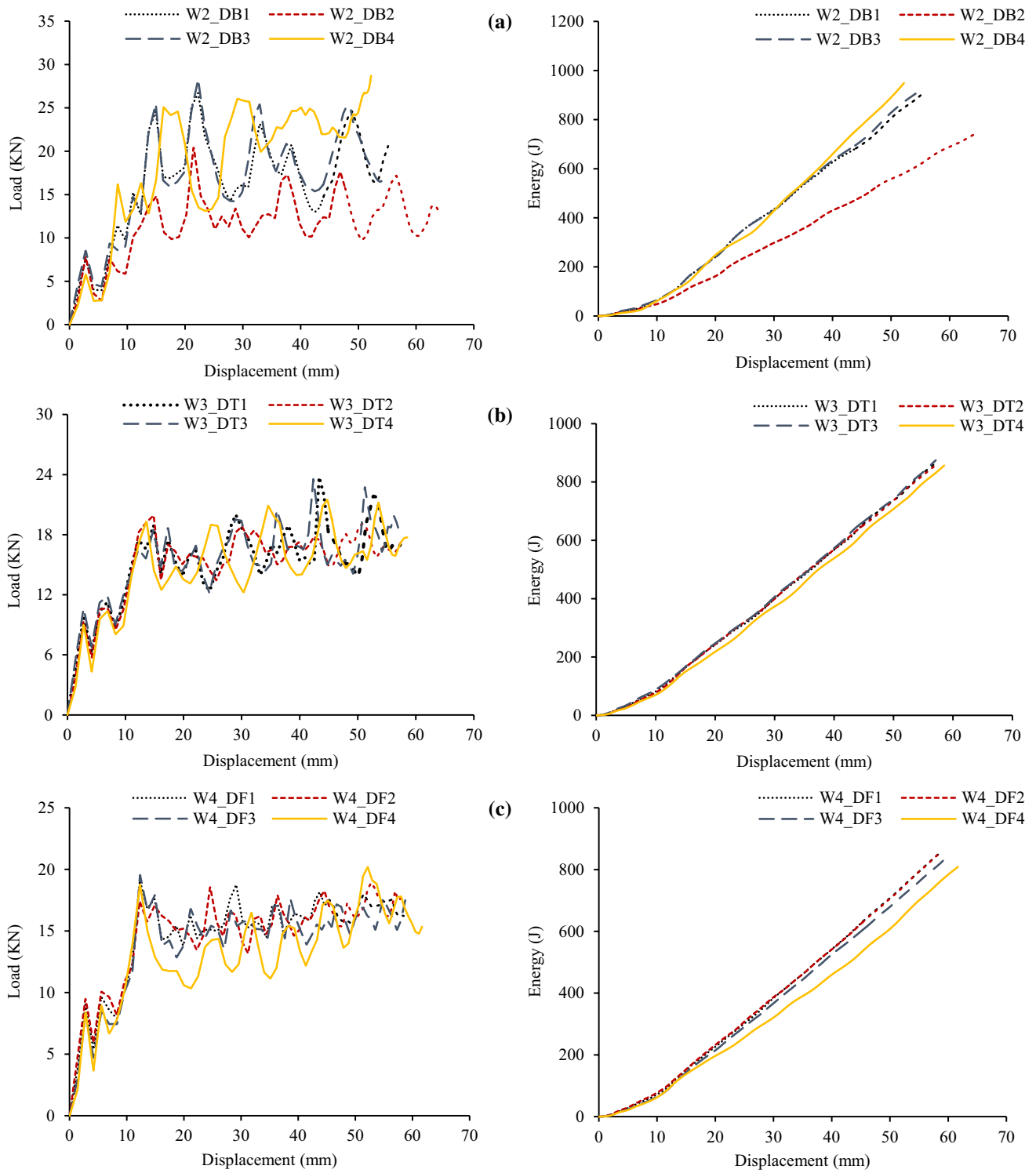


Fig. 13 Load–displacement and energy–displacement plot of: **a** double-, **b** triple- and **c** four-layered frusta tube at 40 kg impactor mass

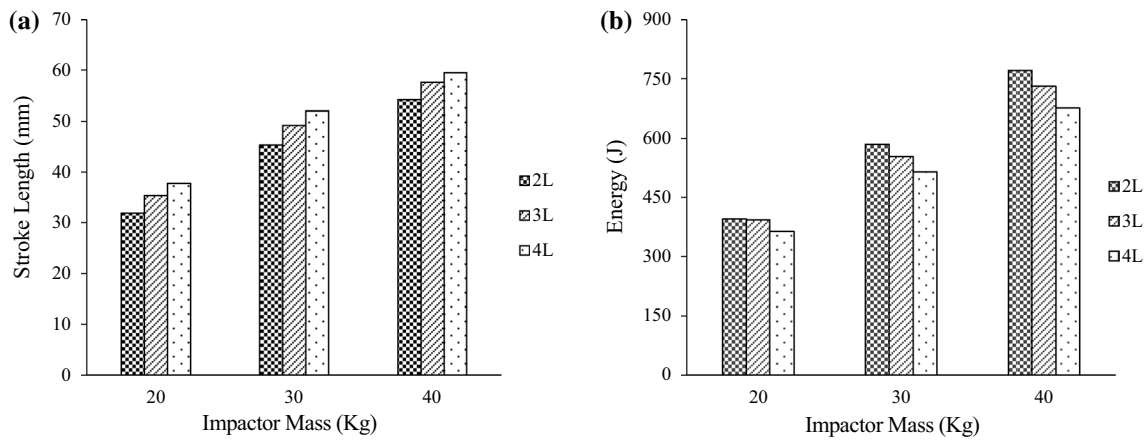


Fig. 14 Comparison of **a** stroke length and **b** energy absorption with the variation of impactor mass and number of layers

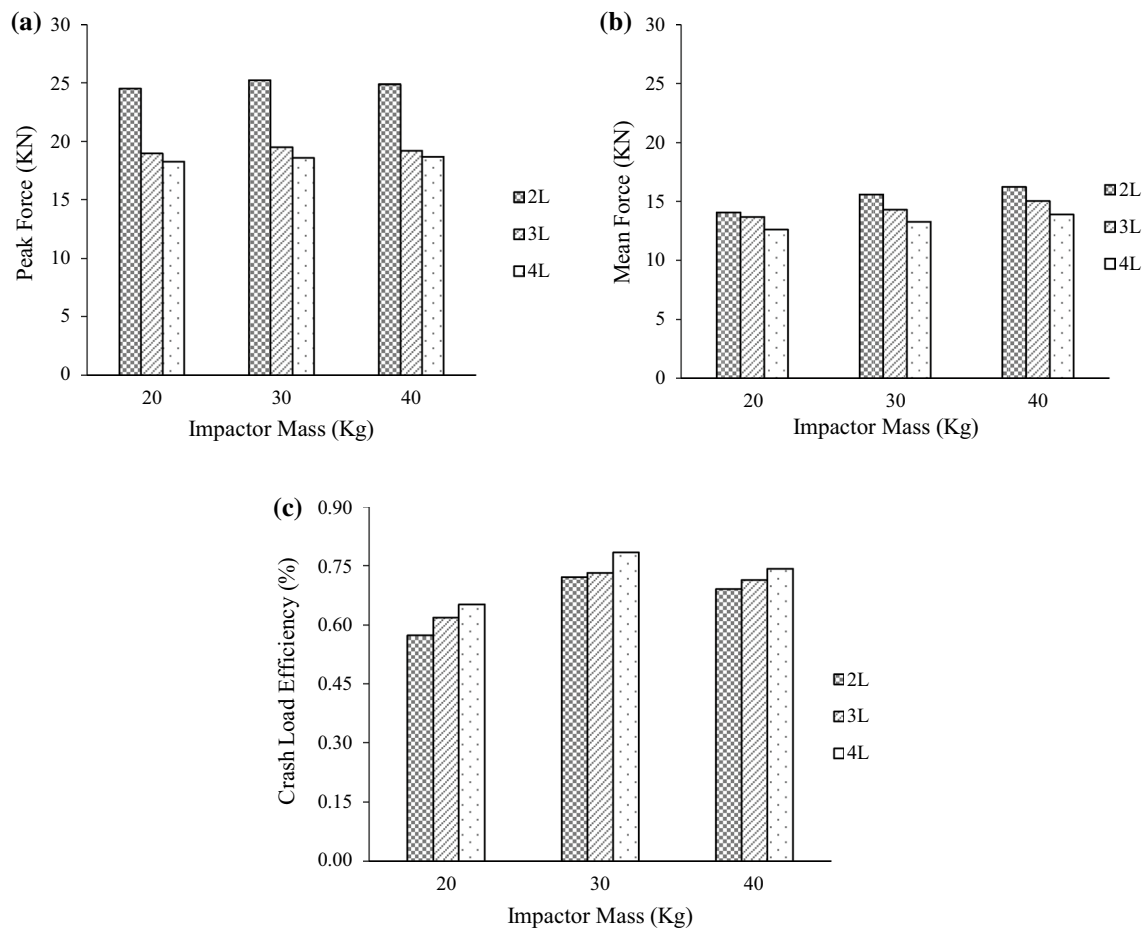


Fig. 15 Comparison of **a** peak force, **b** mean force and **c** crash load efficiency with the variation of impactor mass and number of layers

Acknowledgements Not applicable

Authors' contribution VP contributed to writing—original draft, investigation, data curation, visualization, investigation, funding acquisition,

conceptualization and methodology. GT contributed to review and editing, formal analysis, visualization, conceptualization and methodology. RD contributed to formal analysis, supervision, and conceptualization.

Funding Not applicable.

Declarations

Conflict of interest The authors declare no conflict of interest.

Availability of data and material All data are generated and analyzed during the study.

References

- Lu G, Yu T (2003) Energy absorption of structures and materials. Elsevier, Woodhead Publishing Limited, PA
- Wang B, Lu G (2002) Mushrooming of circular tubes under dynamic axial loading. *Thin-walled Struct* 40(2):167–182. [https://doi.org/10.1016/S0263-8231\(01\)00057-X](https://doi.org/10.1016/S0263-8231(01)00057-X)
- Liu Y, Day ML (2008) Bending collapse of thin-walled circular tubes and computational application. *Thin-Walled Struct* 46(4):442–450. <https://doi.org/10.1016/j.tws.2007.07.014>
- Al GD, Limam A (2004) Experimental and numerical investigation of static and dynamic axial crushing of circular aluminum tubes. *Thin-Walled Struct* 42(8):1103–1137. <https://doi.org/10.1016/j.tws.2004.03.001>
- DiPaolo BP, Monteiro PJ, Gronsky R (2004) Quasi-static axial crush response of a thin-wall, stainless steel box component. *Int J Solids Struct* 41(14):3707–3733. <https://doi.org/10.1016/j.ijsolstr.2004.02.031>
- Rusinek A, Zaera R, Forquin P, Klepaczko JR (2008) Effect of plastic deformation and boundary conditions combined with elastic wave propagation on the collapse site of a crash box. *Thin-Walled Struct* 46(10):1143–1163. <https://doi.org/10.1016/j.tws.2008.01.009>
- Langseth M, Hopperstad O (1996) Static and dynamic axial crushing of square thin-walled aluminium extrusions. *Int J Impact Eng* 18(7–8):949–968. [https://doi.org/10.1016/S0734-743X\(96\)00025-5](https://doi.org/10.1016/S0734-743X(96)00025-5)
- Gupta NK, Gupta SK (1993) Effect of annealing, size and cut-outs on axial collapse behaviour of circular tubes. *Int J Mech Sci* 35(7):597–613. [https://doi.org/10.1016/0020-7403\(93\)90004-E](https://doi.org/10.1016/0020-7403(93)90004-E)
- Gupta NK (1998) Some aspects of axial collapse of cylindrical thin-walled tubes. *Thin-Walled Struct* 32(1–3):111–126. [https://doi.org/10.1016/S0263-8231\(98\)00029-9](https://doi.org/10.1016/S0263-8231(98)00029-9)
- Daneshi GH, Hosseinipour SJ (2002) Elastic–plastic theory for initial buckling load of thin-walled grooved tubes under axial compression. *J Mater Process Technol* 125–126:826–832. [https://doi.org/10.1016/S0924-0136\(02\)00383-7](https://doi.org/10.1016/S0924-0136(02)00383-7)
- Daneshi GH, Hosseinipour SJ (2002) Grooves effect on crashworthiness characteristics of thin-walled tubes under axial compression. *Mater Des* 23(7):611–617. [https://doi.org/10.1016/S0261-3069\(02\)00052-3](https://doi.org/10.1016/S0261-3069(02)00052-3)
- Mokhtarnezhad F, Salehghaffari S, Tajdari M (2009) Improving the crashworthiness characteristics of cylindrical tubes subjected to axial compression by cutting wide grooves from their outer surface. *Int J Crashworthiness* 14(6):601–611. <https://doi.org/10.1080/13588260902896466>
- Karagiozova D, Jones N (2001) Dynamic effects on buckling and energy absorption of cylindrical shells under axial impact. *Thin-Walled Struct* 39(7):583–610. [https://doi.org/10.1016/S0263-8231\(01\)00015-5](https://doi.org/10.1016/S0263-8231(01)00015-5)
- Nagel GM, Thambiratnam D (2004) A numerical study on the impact response and energy absorption of tapered thin-walled tubes. *Int J Mech Sci* 46(2):201–216. <https://doi.org/10.1016/j.ijmecsci.2004.03.006>
- Reid SR, Reddy TY (1986) Static and dynamic crushing of tapered sheet metal tubes of rectangular cross-section. *Int J Mech Sci* 28(9):623–637. [https://doi.org/10.1016/0020-7403\(86\)90077-9](https://doi.org/10.1016/0020-7403(86)90077-9)
- Nia AA, Hamedani JH (2010) Comparative analysis of energy absorption and deformations of thin walled tubes with various section geometries. *Thin-Walled Struct* 48(12):946–954. <https://doi.org/10.1016/j.tws.2010.07.003>
- Prasad GLE, Gupta NK (2005) An experimental study of deformation modes of domes and large-angled frusta at different rates of compression. *Int J Impact Eng* 32(1–4):400–415. <https://doi.org/10.1016/j.ijimpeng.2004.12.001>
- El-Sobky H, Singace AA, Petsios M (2001) Mode of collapse and energy absorption characteristics of constrained frusta under axial impact loading. *Int J Mech Sci* 43(3):743–757. [https://doi.org/10.1016/S0020-7403\(00\)00036-9](https://doi.org/10.1016/S0020-7403(00)00036-9)
- Kim HS (2002) New extruded multi-cell aluminum profile for maximum crash energy absorption and weight efficiency. *Thin-Walled Struct* 40(4):311–327. [https://doi.org/10.1016/S0263-8231\(01\)00069-6](https://doi.org/10.1016/S0263-8231(01)00069-6)
- Mahmoodi A, Shojaeefard M, Googarchin HS (2016) Theoretical development and numerical investigation on energy absorption behavior of tapered multi-cell tubes. *Thin-Walled Struct* 102:98–110. <https://doi.org/10.1016/j.tws.2016.01.019>
- Gan N, Yao S, Dong H, Xiong Y, Liu D, Pu D (2018) Energy absorption characteristics of multi-frusta configurations under axial impact loading. *Thin-Walled Struct* 122:147–157. <https://doi.org/10.1016/j.tws.2017.10.011>
- Kashani MH, Alavijeh HS, Akbarshahi A, Shakeri M (2013) Bitubular square tubes with different arrangements under quasi-static axial compression loading. *Mater Des* 51:1095–1103
- Goel MD (2015) Deformation, energy absorption and crushing behavior of single-, double-and multi-wall foam filled square and circular tubes. *Thin-Walled Struct* 90:1–11. <https://doi.org/10.1016/j.tws.2015.01.004>
- Patel V, Tiwari G, Dumpala R (2019) Effect of eccentric loading on energy absorbing circular cap and open end frusta tube structures. *Vacuum* 166:356–363. <https://doi.org/10.1016/j.vacuum.2018.10.056>
- Patel V, Tiwari G, Dumpala R (2020) Crashworthiness analysis of multi-configuration thin walled co-axial frusta tube structures under quasi-static loading. *Thin-Walled Struct* 154:106872. <https://doi.org/10.1016/j.tws.2020.106872>
- Chahardoli S, Nia AA (2017) Experimental and numerical investigations on collapse properties of capped-end frusta tubes with circular triggers under axial quasi-static loading. *Int J Mech Sci* 134:545–561. <https://doi.org/10.1016/j.ijmecsci.2017.10.037>

Publisher's Note Springer Nature remains neutral with regard to jurisdictional claims in published maps and institutional affiliations.